

# Characterization of biomaterials with reference to biocompatibility dedicated for patient-specific finger implants

ADAM BYRSKI<sup>1</sup>, MAGDALENA KOPERNIK<sup>2\*</sup>, ŁUKASZ MAJOR<sup>1</sup>, KATARZYNA KASPERKIEWICZ<sup>3</sup>,  
MARCIN DYNER<sup>4</sup>, JUERGEN M. LACKNER<sup>5</sup>, DAVID B. LUMENTA<sup>6</sup>, ROMAN MAJOR<sup>1</sup>

<sup>1</sup> Institute of Metallurgy and Materials Science, Polish Academy of Sciences, Kraków, Poland.

<sup>2</sup> AGH University of Krakow, Kraków, Poland.

<sup>3</sup> Institute of Biology, Biotechnology and Environmental Protection, Faculty of Natural Sciences,  
University of Silesia in Katowice, Katowice, Poland

<sup>4</sup> Faculty of Science and Technology, Jan Długosz University in Częstochowa, Częstochowa, Poland.

<sup>5</sup> JOANNEUM RESEARCH Forschungsgesellschaft mbH, MATERIALS – Institute for Sensors,  
Photonics and Manufacturing Technologies, Niklasdorf, Austria.

<sup>6</sup> Research Unit for Digital Surgery, Division of Plastic, Aesthetic and Reconstructive Surgery,  
Department of Surgery, Medical University of Graz, Austria.

*Purpose:* The research was focused on determining basic mechanical properties, surface, and phase structure taking into consideration basic cytotoxicity analysis towards human cells. *Methods:* Biological tests were performed on human C-12302 fibroblasts cells using 3D-printed Ti6Al4V alloy (Ti64), produced by laser-based powder bed fusion (LB-PBF) and Alumina Toughened Zirconia 20 (ATZ20), produced by lithography-based ceramic manufacturing (LCM). Surface modifications included electropolishing and hydroxyapatite or hydroxyapatite/zinc coating. Structure analysis was carried out using a variety of techniques such as X-Ray diffraction, scanning electron microscopy (SEM), transmission electron microscopy (TEM) and confocal laser scanning microscopy (CLSM), followed by mechanical properties evaluation using nanoindentation testing. *Results:* Samples subjected to surface modifications showed diversity among surface and phase structure and mechanical properties. However, the cytotoxicity towards tested cells was not significantly higher than the control. Though, a trend was noted among the materials analysed, indicating that HAp/Zn coating on Ti64 and ATZ20 resulted in the best biological performance increasing cell survivability by more than 10%. *Conclusions:* Hydroxyapatite coating on Ti64 and ATZ20 resulted in the best biological properties. Tested materials are suitable for *in vivo* toxicity testing.

*Key words:* laser based-powder bed fusion, lithography-based ceramic manufacturing, bone implant, cytotoxicity, micromechanical properties

## 1. Introduction

Bone defects greatly affect human life and well-being. Bone tissue has the ability to self-repair and regenerate in response to damage. However, huge bone defects occurring after tumor resection or traumatic fracture require external support in order to maintain the organ functionality [32]. A finger amputation may result in failed replantation due to severe damage. In such cases, surgical reconstruction is only possible by an autograft transplantation, e.g., toe-to-hand transfer,

leading to impairment at the foot site. Some motion functional restoration is also possible by the bone-anchored silicone prosthesis even as lacking sensitivity [41]. Current research focuses on alternatives for surgical reconstruction by patient-specific, durable, biomimetic, bioactive and antibacterial implants for the reconstruction of lost bone and joints [37]. Reconstruction of the hard tissue is planned by applying metal and ceramics additive manufacturing (AM, “3D printing”). Research focuses on selective laser melting (SLM) process development (optimization of laser power scanning and powder layer properties) to achieve defined

\* Corresponding author: Magdalena Kopernik, AGH University of Krakow, al. Mickiewicza 30, 30-059 Kraków, Poland. Phone: +48 12 617 51 26, e-mail: kopernik@agh.edu.pl

Received: November 21st, 2022

Accepted for publication: February 22nd, 2023

roughness and minimize defects from melting (pores, oxide inclusions, etc.), which is especially important for the planned sub-mm sized structures, e.g., as niches with healthy bone [30], [36]. Due to ~25% lower elastic modulus to prevent stress shielding, bone degradation, and mid-/long-term implant loosening, the non-cytotoxic Ti-15Mo-5Zr-3Al alloy is planned to be used instead of the state-of-the-art Ti6Al4V [47]. However, for commercial reasons, availability and universality of materials used, Ti6Al4V alloy was chosen for the purposes of the work presented here.

The design of artificial finger joint implants will overcome the problem of the strong ossification tendency which occurs in the case of implants made of pyrolytic carbon or CoCr-based alloys applied in reconstruction of state-of-the-art gold-standard. Based on dental implant know-how (i.e., tooth crowns), the goal is a development of ultra-dense, tough, hard and especially non-osteoconductive ZrO<sub>2</sub>-Al<sub>2</sub>O<sub>3</sub> composite ceramics (Alumina Toughened Zirconia, ATZ) deposited by AM (additive manufacturing) [6], [26], [49] with lithography-based ceramic manufacturing (LCM), including post-annealing of as-synthesised parts and polishing to patient-specific developed joints. Key issues for long-term functionality of biomaterial-based reconstruction of hard tissue are based on surgical demands: (1) perfect integration of bone substituting metal to the surrounding bone tissue (a) without loosening due to stress shielding at the interface and (b) with protection against bacterial inflammation (antimicrobial properties and formation of vascularized bone tissue (ossification)) even months to years after the injury; (2) biomimetic finger joints based on non-wearing materials without ossification tendency to prevent loss of motion function. In detail, research envisages following innovations on additive manufacturing (AM, “3D printing”) and bioactive coatings for hard tissue reconstruction: (i) AM technologies for mechanically durable, patient-specific hard tissue implants with: a) fatigue- and corrosion-resistant bone substitute scaffolds of high elastic Ti-15Mo based alloys achieved by selective laser melting (SLM) with final isostatic pressing; b) wear-resistant, ultra-smooth and non-osteoconductive finger-joint implants of tough lithography-based ZrO<sub>2</sub>-Al<sub>2</sub>O<sub>3</sub> ceramics. (ii) Biomimetic CAD-CAM implant design from CT images with scalable templates for predominating bone defects. Special focus is laid on directional adaptation of implant tension, bending and torsion elasticity to bone (= 4D printing) to prevent stress shielding and loosening at the screwing site to (metacarpal) bone, thin subsurface bionic sub-mm pore structure for bone anchoring. (iii) Optimal bioactivity: anti-microbial pro-

tection over >20 weeks and fast, targeted neoformation of vascularized bone on Ti-15Mo surfaces within the patient’s own body as “bioreactor” (safest tissue engineering approach), achieved by bioresorbable, osteoinductive Zn doped hydroxyapatite coatings (HAp) with high adhesion using novel “mini-torch” atmospheric pressure plasma spray deposition (APPD) at low temperature to prevent distortion of small implants. Future research will focus on development of implants characterized by combination of high hardness and toughness, exact physiological free-form surface shape and low roughness. It is necessary to minimize wear even in conditions with micro-sized bone particles from surrounding ossification as third body.

As a basis for future fast adaptation of this complex tissue substitution to the patients’ needs which has to be performed with proper accuracy already during surgical planning, the research is definitely necessary in the field of elaboration of easily applicable CAD (Computer Aided Design) templates from CT (computed tomography) scans even for experienced surgeons. Based on the trend in patient-tailored implant design, these advanced templates will be a key element in transferring this procedure into every day of surgical rooms.

Vascularization in and around implant scaffolds during osseointegration to use the patient’s immune system is a good enough defense against bacteria (i.e., *S. aureus*, *E. coli*), which otherwise colonize – even weeks after surgery – especially on the implant surface and form hardly treatable biofilms [23]. Bioresorbable coatings supporting bone neoformation like hydroxyapatite (HAp) are well established in joint arthroplasty. However, the applied state-of-the-art technologies (mainly thermal and plasma spraying) can hardly cope when applied into small-sized, heat and distortion sensitive implants like the planned finger bone substitutes [18]. The drawbacks in such case are low adhesion and non-controlled bioresorption aggravated by high thermal load and limited control of phase formation. Instead of non-resorbable crystalline phase, an amorphous, bioresorbable phase forms at the interface due to high cooling rate. Eventually it results in catastrophic failure within wet *in vivo* surrounding by rapid coating delamination [22]. Atmospheric pressure plasma deposition (APPD) systems (“mini torch” plasma spraying) have the potential for overcoming these limitations. The “mini torch” spraying makes it possible to control the phase formation using the localization of the energy input and plasma pre/post-annealing [25].

Optimized powder size (size distribution, shape and composition, stabilizing dopants) is a further key for

chemical- and phase-graded HAp with both long-term stable crystalline adhesion layers and amorphous top layers [3], [11], [39]. Additionally, introduction of Zn salt via aerosols into HAp makes it medically safe [28], [44]. The aim is to obtain intermediate antimicrobial protection for up to 20 weeks after implantation, in which vascularized bone tissue should be already formed on the implant surface triggered by bioresorption of amorphous, osteoinductive HAp. This is the critical, long time for biofilm formation [24], which is difficult to treat by oral antibiotic drugs (with low dose at the implant site) [31]. Furthermore, Zn is in contrast to currently used antimicrobial Ag (formation of microbial resistances) [12] mandatory for bone formation (osteoconductive), as it speeds up bioresorption. However, it is rarely applied in commercial medical coatings as of yet [9].

The objective of this work was to determine the impact of surface modifications (electropolishing, anodisation, HAp and HAp/Zn coating) on phase composition, mechanical properties and biocompatibility of Ti6Al4V (Ti64) and Alumina Toughened Zirconia 20

(ATZ20) ceramic materials and their selection for the practical application (finger implants).

## 2. Materials and methods

### 2.1. Material manufacturing

The Alumina Toughened Zirconia 20 (ATZ20) samples were sintered at 1550 °C for 2 h with layer thickness of 25 µm. The printing parameters are shown in Table 1.

The Medical alloy Ti6Al4V samples were 3-D printed (LB-PBF, laser based-powder bed fusion) using stripe power of 280 W, stripe speed of 1200 mm/s, stripe distance of 0.14 mm and layer thickness of 30 µm. Heat treatment of (Ti64) was carried out in argon furnace at 650 °C for 2 hours. All samples were in the shape of discs with diameter of 13 mm and height of 3 mm. The substrates were prepared by Lithoz company, the project partner.

Table 1. Alumina Toughened Zirconia 20 printing parameters

Lateral (XY) shrinking compensation	Build direction (Z) shrinking compensation	Angle of rotation start [rotations]	Angle of rotation general [rotations]	Rotation speed [°/s]	Settling time start [s]	Settling time general [s]	
1.35	1.36	2	2	100	90	8	
Tilt up speed start [°/s]	Tilt up speed general [°/s]	Backlight exposure time [s]	Settling time backlight layer [s]	Energy start [mJ/cm <sup>2</sup> ]	Energy general [mJ/cm <sup>2</sup> ]	Tilt down speed start [°/s]	Tilt down speed general [°/s]
8	15	2	90	250	200	3	12

Table 2. Coating process parameters

Sample	Plasma gas	Plasma Stream [L/mm]	Nozzle – substrate distance [mm]	Plasma stream current intensity [A]	Platform velocity [mm/s]	Coating runs	
Ti64	Ar 5.0	10	30	270	300	5 (gridded)	
ATZ20 (activation)	Ar 5.0	10	35	300	300	2 (linearly)	
ATZ20 (coating)	Ar 5.0	10	35	400	300	2 (linearly)	
Sample	HMDSO (adhesion promoter)	Powder	Internal gas	Gas stream internal [L/min]	Intel powder feeder	Powder feeder [%]	Powder Stream [g/min]
Ti64	No	HAp	Ar 5.0	~5	1.6	80	~2
ATZ20 (activation)	No	–	Ar 5.0	~5	1.6	65	~1
ATZ20 (coating)	No	HAp	Ar 5.0	~5	1.6	65	~1

The first rout of the surface modification was done by deposition of the hydroxyapatite (HAp) coating. Prior to coating, samples were washed in ethanol and dried. HAp powder (50 g containing 0.1 g Aerosil 8200, MF/17-37198, Medicoat, Switzerland) with particle size of 25  $\mu\text{m}$  was used. Flat tungsten anode with a nozzle diameter of 4 mm was used. Prior to coating, ATZ20 sample was activated using hexamethyldisiloxane (HMDSO). Coating parameters are shown in Table 2.

The second surface treatment was carried out by an anodic oxidation performed using current of 2.25 A and voltage of 28 V. Detailed procedure can be found elsewhere [1].

The third option was accomplished by electro-polishing. As-synthesised samples were deoxygenated in the 10%  $\text{HNO}_3$  (438073, Sigma-Aldrich, USA) / 4% HF (695068, Sigma-Aldrich, USA) mixture for 10–15 seconds. Heat-treated samples were deoxygenated for longer time, i.e.,  $\sim 60$  seconds, until the color faded away. The deoxygenated samples were placed in 15  $\text{dm}^3$   $\text{CH}_3\text{OH}$  (34860, Sigma-Aldrich, USA) / 1350  $\text{cm}^3$  98%  $\text{H}_2\text{SO}_4$  (258105, Sigma-Aldrich, USA) mixture bath, with the voltage of 15 V and temperature of  $-20^\circ\text{C}$  for 10 minutes. Detailed protocol for polishing procedure can be found elsewhere [48].

## 2.2. Surface topography, structure and microstructure assessment

Surface images of tested samples were taken with digital light microscope SmartZoom 5 (Carl Zeiss, Germany) equipped with a PlanApo D 5 $\times$ /0.3 FWD (Free Working Distance) 30 mm objective, at magnification of  $\times 100$  and  $\times 300$ . The surface roughness ( $R_a$ ,  $R_z$ ) parameters of each sample were determined using confocal laser scanning microscope (Exciter 5, Carl Zeiss, Germany) equipped with a EC Plan-Neofluar 5 $\times$ /0.16 objective with Z-stack mode, in accordance to ISO 4287. Images were analysed using ZEN 2008 v5.0.0.267, (Carl Zeiss, Germany). For scanning electron microscopy observations and TEM, lamella preparation a DualBeam SCIOS II scanning microscope (ThermoFisher, USA), equipped with FEG (Field Emission Gun) electron gun (30 kV) and an ion gun was used. For SEM images Everhart–Thornley Detector (ETD) using SE (Secondary Electron) mode, acceleration voltage of 2.00 kV and a working distance (WD) of 3 mm was used.

Microstructure studies were performed using a Themis high-resolution transmission microscope (Thermo-

Fisher, USA) equipped with FEG electron gun (200 kV), a HAADF detector for scanning transmission electron microscopy (STEM) observations and integrated X-ray spectrometer for the analysis of the chemical composition (EDAX, USA).

Qualitative (identification) phase analysis was carried out using a Bruker D8 Discover (Bruker, USA) with  $\text{CoK}\alpha$  filtered radiation. Diffractograms were analysed using DiffraCeva v3.0 (Bruker, USA) and PDF-4+ 2022 base (ICDD, USA).

## 2.3. Mechanical properties

Tests were carried out using the Step 500 (Anton Paar, Austria) which is equipped with the Nanoindenter NHT<sup>3</sup> (nano hardness tester) and MCT<sup>3</sup> (micro combi tester) modules, equipped with a system for collecting and archiving measurement results. Nanoindenter NHT<sup>3</sup> is a precise device designed to determine the mechanical properties of materials and thin layers in a nanometric scale. NHT<sup>3</sup> meets the requirements of the ASTM-E2546 standard for nano-hardness testers, while the MCT<sup>3</sup> module complies with ASTM: C1624, E2546, G171 and ISO: 14577, 20502, 27307. The micromechanical properties were determined on the basis of material deformation, as a result of indentation of the sample with an indenter to which a certain load is applied. The value of the loading force and the penetration depth of the indenter blade were recorded continuously during the entire cycle (loading and unloading). Based on the load curve vs. displacement, such properties as: hardness, Young's modulus, creep time, fracture toughness were determined. Using minimal forces loading the indenter, it is possible to perform measurements at depths of several hundred nanometers, which is particularly important when testing thin layers, where the influence of the substrate on the determined properties should be eliminated. Nanoindentation tests: hardness (HiT), Vickers hardness (HV), and Young's modulus (EiT) were performed using Berkovich tip, and load of 0.5 N. For each test, a total of 10 measurements from 3 samples of each type were taken.

## 2.4. Cytotoxicity

Direct cytotoxicity tests were conducted using Normal Human Dermal Fibroblasts (NHDF, Promocell, Germany) C-12302 cells in accordance with ISO 10993-5. Prior to material testing, cells were incubated using

Fibroblast Growth Medium (C-23020, Promocell, Germany), supplemented with Antibiotic Antimycotic Solution (A5955, Sigma-Aldrich, USA) and enriched with Fibroblast Growth Medium 2 Supplement Mix (C-39325 Promocell, Germany) and detached using StableCell Trypsin Solution (T2610, Sigma-Aldrich, USA). Cells were cultured according to manufacturer's manual and ISO standard. A total of 3 specimens per sample were tested. Specimens were placed in 24-well cell culture plates, with a cell diameter of 15. mm. Cell concentration was  $10^5$  cells/mL. Cells were incubated at 37 °C and 5% CO<sub>2</sub> for 24 hours. Out of 3 samples, 2 representative samples were selected for further testing. Live and necrotic cells were evaluated with confocal laser scanning microscopy (Exciter 5, Carl Zeiss, Germany) equipped with a EC Plan-Neofluar 5×/0.16 objective, with Z-stack mode using propidium iodide (P4170, Sigma-Aldrich, USA) (staining dead cells red) and MitoTracker Green (M7514, ThermoFisher, USA) (marking live cells green). Staining was performed according to the manufacturer's instructions. Cells were fixed using 4% formaldehyde (114321734, Pol-Aura, Poland) solution. Images were analysed using ZEN 2008 v5.0.0.267, (Carl Zeiss, Germany). The software is equipped with the colocalization function that counts pixels allowing comparison between green and red channel pixel number. The more propidium iodide excitation, the greater the likelihood that cells located on the surface of the biomaterial are dead. Percentage of live cells was calculated by dividing number of green pixels by the number of green and red pixels in each photography taken. A total of 10 images per sample were taken. Cell culture supernatant was collected and evaluated for lactate dehydrogenase levels using CytoTox 96<sup>®</sup> Non-Radioactive Cytotoxicity Assay Protocol (Promega, USA) using Cobas Integra 400 analyser (Roche, Switzerland). Results are presented as enzyme unit per liter. A total of 4 measurements per each sample were performed. As the positive control material, uncoated as-synthesised Ti64 was used. As the negative control, a blank cell culture well was used.

## 2.5. Statistical analysis

Statistical significance was evaluated using STATISTICA 13.3 (StatSoft, Tulsa, USA). An analysis of variance (ANOVA) followed by a post-hoc least significant difference (LSD) test was used to estimate any significant effect between groups. Differences between treatments with *p*-value below 0.05 were considered statistically significant.

## 3. Results

### 3.1. Surface topography and microstructure analysis

#### 3.1.1. Digital microscopy

Macro-scale images of materials surface topography are shown in Fig. 1. The surface of as-synthesised Ti64, which is of gray/silver hue (Fig. 1a) becomes colorful after heat treatment due to light interference within the newly formed oxide layer. Hydroxyapatite (HAp) coating is observed as gray (Fig. 1c, d, g and h). Blue color (Fig. 1e) is the result of defined oxide layer thickness which is related to applied voltage of 28 V. "Blurred" surface (Fig. 1f) is the effect of surface etching. Zinc particles in HAp/Zn coating are visible as shimmering spots (Fig. 1d, h).

#### 3.1.2. Confocal laser scanning microscopy

Results of surface topography measurements are presented in Fig. 2. Mean surface roughness (Ra) of uncoated 3D-printed Ti64 varied between 12.2 μm for as-synthesised and 13.4 μm for the annealed sample. The electropolishing significantly lowered mean Ra values to 8.1 μm and 4.38 μm, respectively. The anodisation resulted in significantly increased roughness, i.e., 14 μm for as-synthesised Ti64 and 18.3 μm for annealed Ti64. The HAp coating led to significant lowering of the mean surface roughness to 6.0 μm regardless whether a sample was annealed or not. The HAp/Zn coating lowered Ra value to 4.7 μm. Surface roughness parameters of all ceramic ATZ20 samples varied between 4.7 μm for both untreated and HAp/Zn coated ATZ20 samples and 5.0 μm for HAp coated ones. Differences between all HAp coated samples and uncoated ATZ20 were negligible.

Mean maximum height of the profile (Rz) of uncoated 3D-printed Ti64 varied between 72.3 μm for as-synthesised and 79.1 μm for the annealed sample. The electropolishing significantly lowered mean Rz values to 23.5 μm and 17.4 μm, respectively. The anodisation resulted in significantly increased roughness, i.e., 80. μm for as-synthesised Ti64 and 87.2 μm for annealed Ti64. The HAp coating led to significant lowering of mean maximum height of the profile to 23.5 μm for as-synthesised and 17.4 μm for annealed Ti64. The HAp coating lowered Rz value to 36.7 μm for as-synthesised and 31.6 μm for annealed sample. HAp/Zn coating lowered the Rz of annealed Ti64 to 28.4 μm. Surface roughness parameters of all ceramic

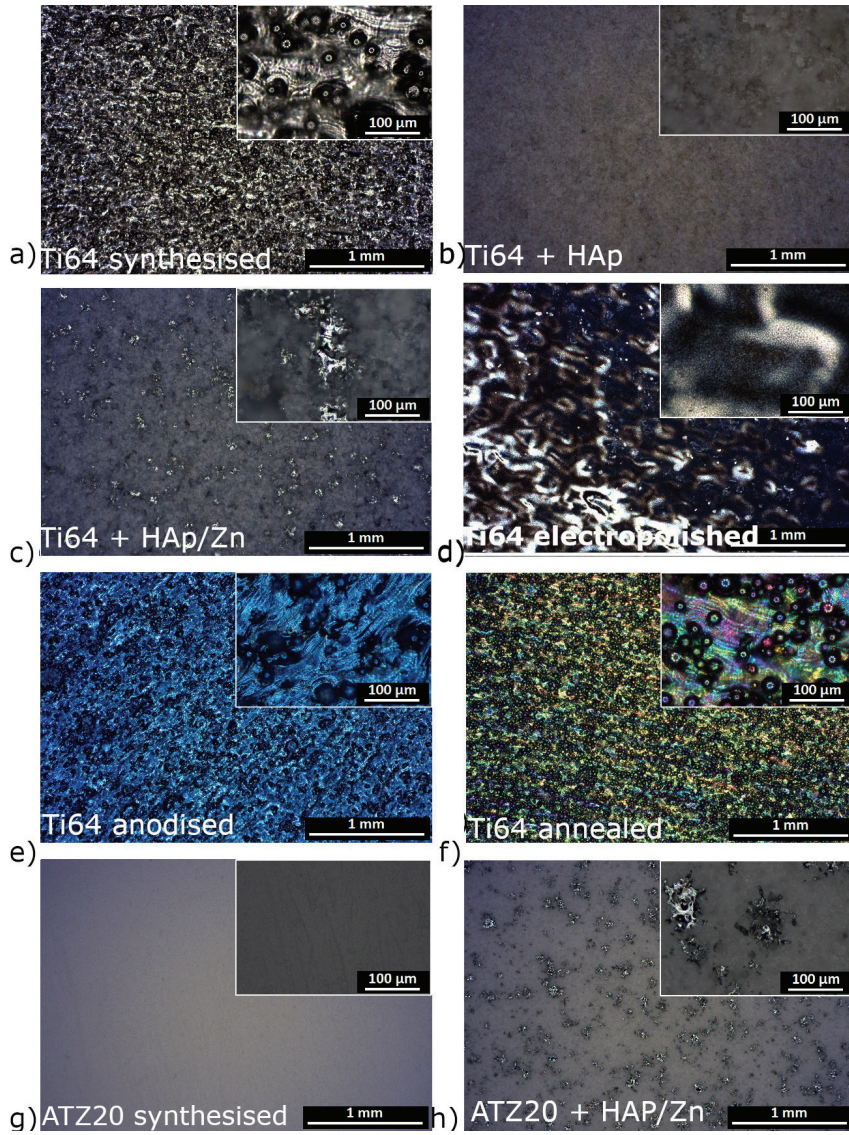


Fig. 1. Digital microscopy images: a) Ti64 as-synthesised, b) Ti64 annealed, c) Ti64 + HAp, d) Ti64 + HAp/Zn, e) Ti64 anodised, f) Ti64 electropolished, g) ATZ20 as-synthesised, h) ATZ20 + HAp/Zn. PlanApo D 5×/0.3, mag. ×100 and ×300

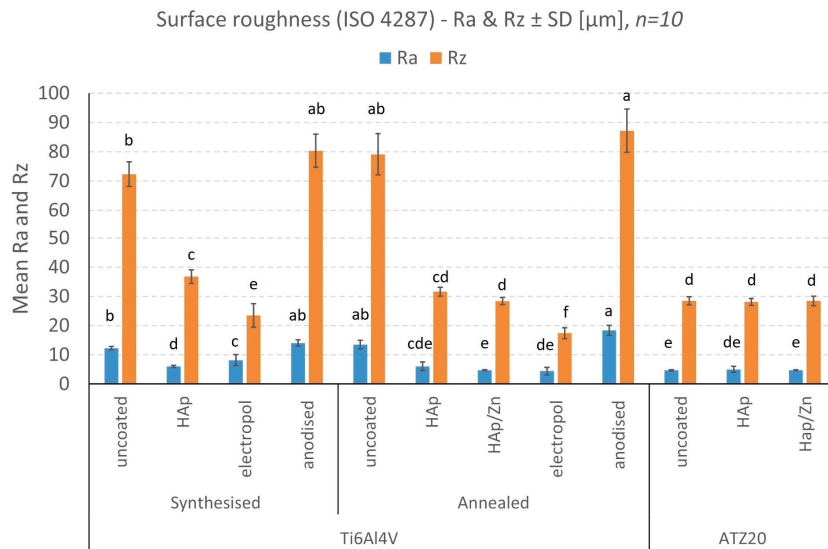


Fig. 2. Surface roughness of tested samples, (ISO 4287) – Ra and Rz ± SD [μm], n = 10, EC Plan-Neofluar 5×/0.16, Z-stack mode

ATZ20 samples varied around  $28.4 \mu\text{m}$  for untreated, HAp and HAp/Zn coated ATZ20 samples. Differences between ATZ20 samples were negligible. Overall, both uncoated and anodized Ti64 samples had significantly higher Rz values compared to the rest of tested samples.

### 3.1.3. Scanning electron microscopy (SEM)

SEM images of the Ti64 and ATZ20 tested samples are shown in Fig. 3. The uncoated (Fig. 3a) surface of 3D-printed Ti64 sample shows residue of melted powder used for a LB-PBF process. Within the presented scope of research at this level of project implementation, the main focus was on performing basic research, i.e., carrying out in-depth structural and microstructural analysis. On the basis of the microstructural studies,

process residues were identified in the structure. The entire cycle of tests, which was carried out, did not show any significant negative impact on biocompatibility, but this defect had to be eliminated in the manufacturing process itself. The consortium partners used more precise mixing during sample preparation. The harsh surface of HAp coated Ti64 (Fig. 3b) corresponds for the HAp deposition on this mineral. The surfaces of anodised (Fig. 3c, d) samples differed from the previous ones showing layers of  $\text{TiO}_2$  as smooth film and islands. Increased number of island structures was found on the annealed surface when compared to the as-synthesised one. The electropolishing (Fig. 3e, f) resulted in smoother surfaces, while the residues in the form of islands are observed as blurred accumulation of material. The SEM analysis confirmed presence of HAp (Fig. 3h) on the ATZ20 surface (Fig. 3g), as well

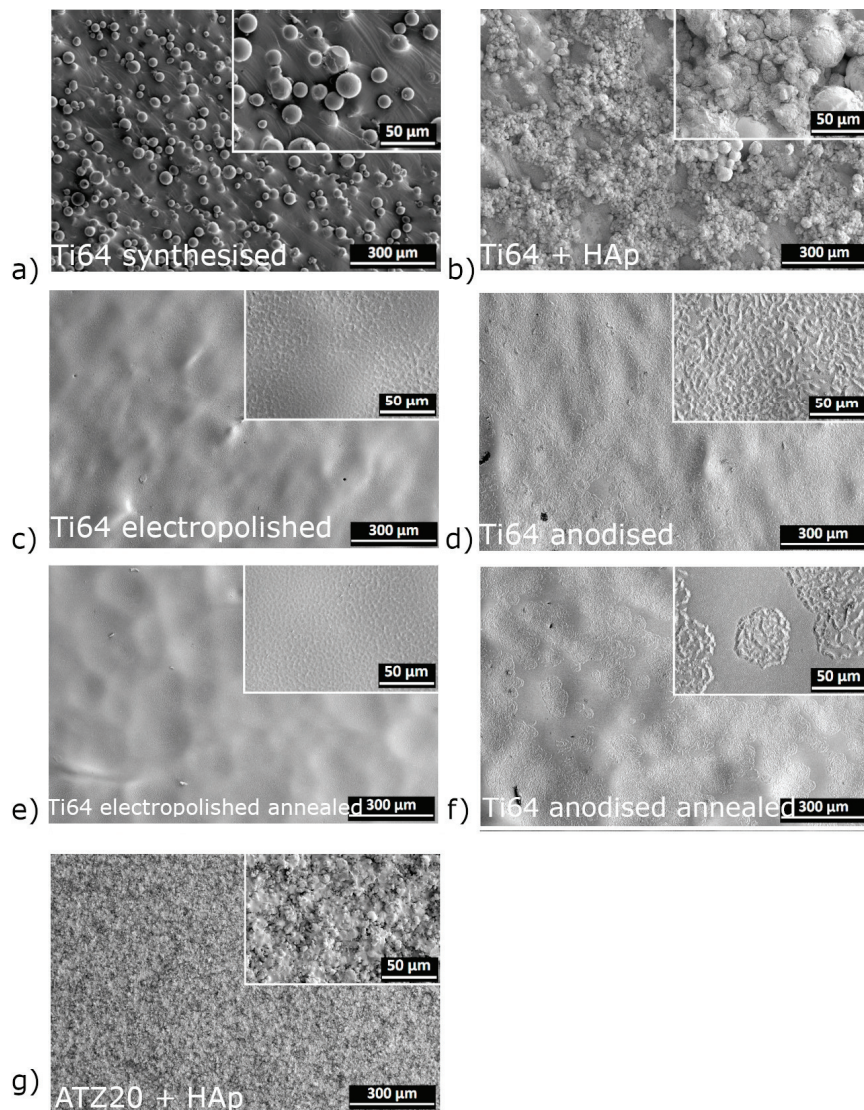


Fig. 3. SEM images of 3D-printed samples: a) Ti64 as-synthesised (uncoated), b) Ti64 + HAp coating, c) Ti64 anodised as-synthesised, d) Ti64 anodised annealed, e) Ti64 electropolished as-synthesised, f) Ti64 electropolished annealed, g) ATZ20 + HAp coating. Acceleration voltage – 2.0 kV, detector – ETD, mode – SE

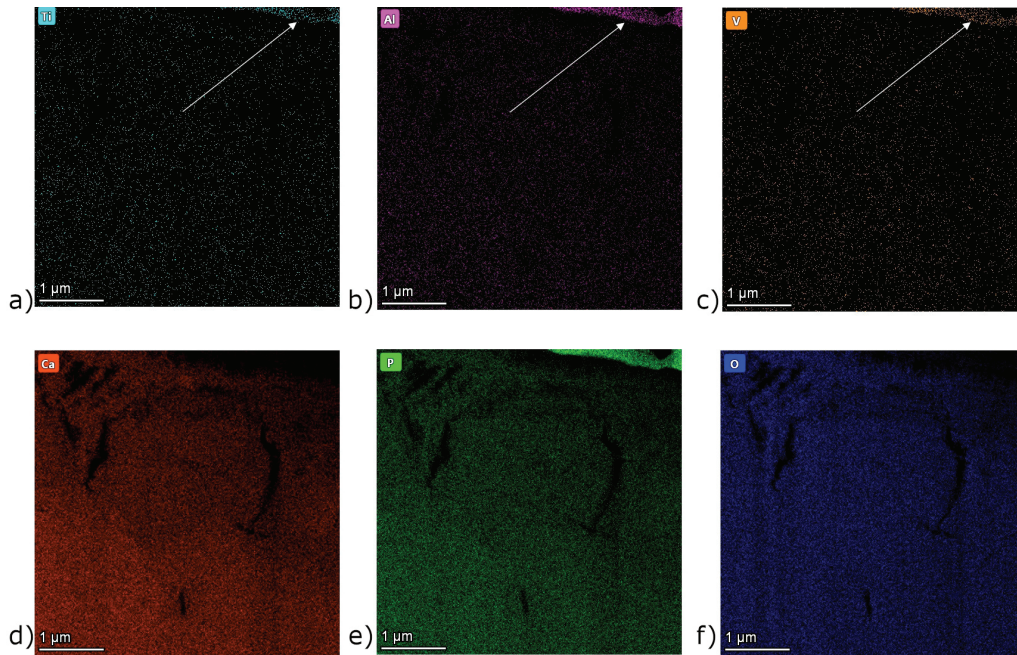


Fig. 4. Results of EDS analysis of HAp coating on the surface of Ti64 – elemental distribution of: a) titanium, b) aluminium, c) vanadium, d) calcium, e) phosphorus, f) oxygen. Arrows mark the uncoated part of the sample. Acceleration voltage – 200 kV

as revealed development of surface cracks. The HAp deposition was confirmed by TEM-EDS mapping of elemental distribution (Fig. 4).

### 3.1.4. Transmission electron microscopy (TEM)

A lamella for TEM investigation was cut out from the space between the smooth surface and the

sphere. It allowed to prove that the columnar growth of crystallites takes place in the direction perpendicular to the surface of the spheres (Fig. 5a). The presence of twins was also noted (Fig. 5b), due to the tendency to twinning in hcp metal crystal lattice. The presence of a thin (~100 nm), fine-crystalline layer was observed at the surface of annealed Ti64 (Fig. 5c).

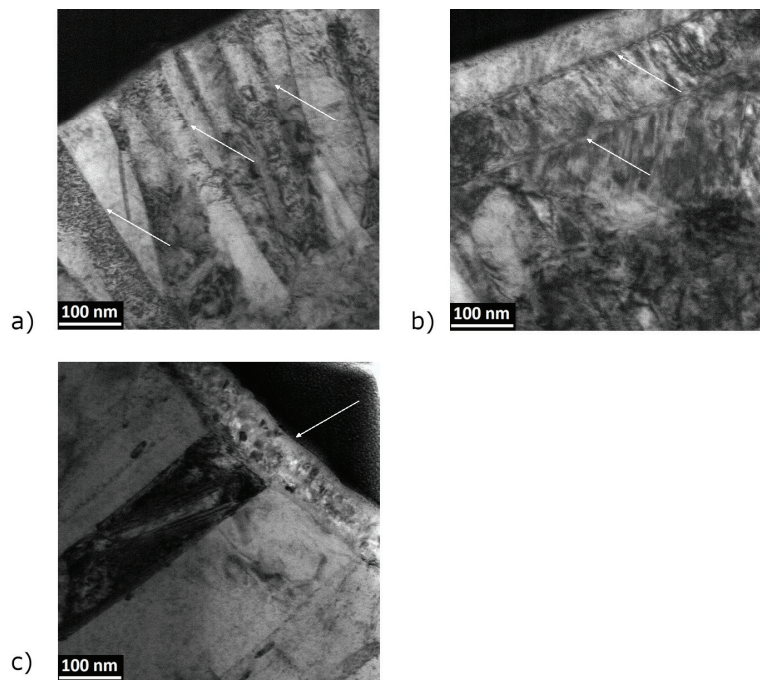


Fig. 5. TEM Bright Field (BF) analysis: a) columnar growth of crystallites, perpendicular to the surface of the spheres (arrows), b) twinning boundaries (arrows), c) fine-crystalline layer on the surface of annealed Ti64 (arrows). Acceleration voltage – 200 kV

### 3.2. X-ray diffraction analysis

XRD (X-Ray Diffraction) patterns of the titanium alloy (Ti64) confirmed the presence of the hexagonal  $\alpha$ -Ti4 phase (Fig. 6, marked green) The presence of tetragonal  $ZrO_2$  and  $\alpha-Al_2O_3$  in the tested material (ATZ20) was also confirmed (Fig. 6, marked black).

### 3.3. Mechanical properties

The results of micromechanical tests are shown in Fig. 7. In the box plot the horizontal line represents the location of the median, the cross shows calculated mean ( $n = 10$ ), the box represents the location of 50% of the results relative to the median, whiskers are results in the range of  $\pm 3 \times$  standard deviation and free

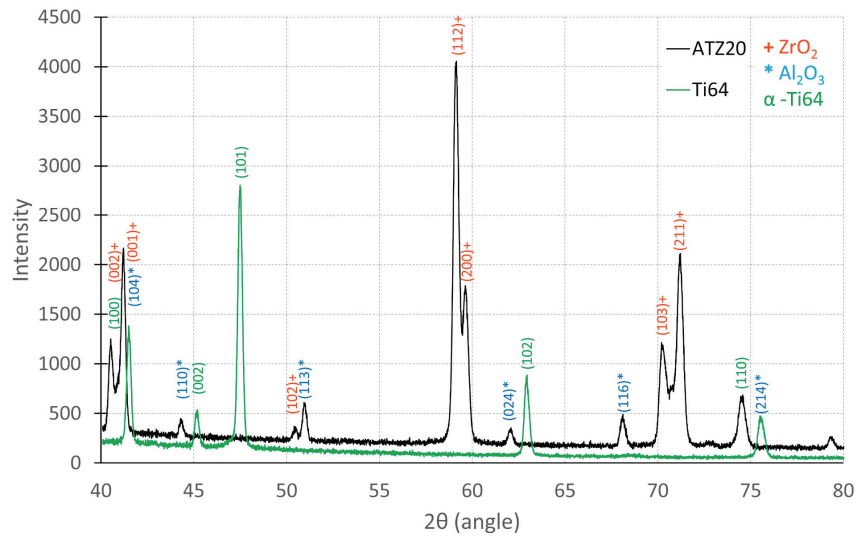


Fig. 6. Green – as-synthesised Ti64 diffractogram – green –  $\alpha$ -Ti6Al4V phase (hexagonal); black – ATZ20 diffractogram; cross (red) –  $ZrO_2$  phase (tetragonal); asterisk (blue) –  $\alpha-Al_2O_3$  phase (rhombohedral)

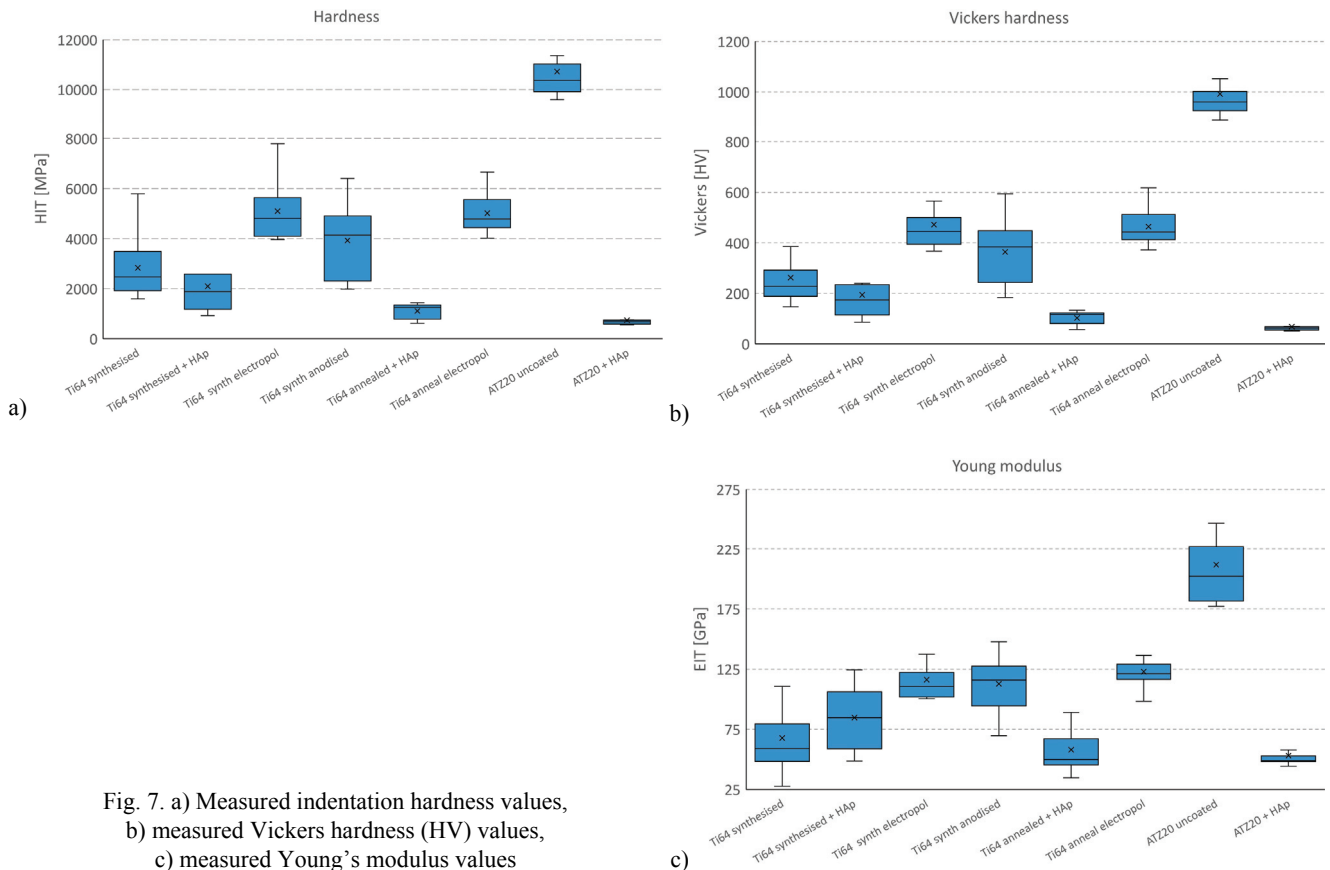


Fig. 7. a) Measured indentation hardness values, b) measured Vickers hardness (HV) values, c) measured Young's modulus values

points stand for extreme values. Indentation hardness (Fig. 7a) values for Ti64 samples generally varied between 700 MPa and 6000 MPa, whereas ATZ20 hardness values were closed to 11000 MPa. Anodised and electropolished samples differed significantly compared to uncoated Ti64. The HAp coating resulted in lowering those values to about 1000 MPa. Vickers hardness (Fig. 7b) values for Ti64 samples generally varied between 100 HV and 600 HV, on the other hand ATZ20 hardness values remained close to 950 HV. For the HAp coating those values varied around 70 HV. In case of Young's modulus (Fig. 7c), its values varied between 25 GPa and 150 GPa for Ti64 samples and around 220 GPa for ATZ20. The HAp coating has shown EiT values from 40 GPa to 75 GPa.

### 3.4. Cytotoxicity

A number of green and red pixels are used to build a co-localization chart in Fig. 8. These results were also visualized as percentage of live cells in Fig. 9. Higher percentage of the latter means that there are more of the live cells than the dead ones. According to ISO 10993-5 material is not cytotoxic if at least 70% of live cells (red reference line) can

be observed. Direct cytotoxicity analysis showed significant diversity among live/dead cells ratio for HAp/Zn coated samples in comparison to the remaining, however, these results were not directly comparable to the measured LDH levels (Fig. 10), most of which were negligibly higher than the reference (~4 U/L) sample.

## 4. Discussion

The performed tests were focused on characterization of the properties of materials produced by additive methods for finger bone implants. The 3D printing technique allows to match the material perfectly for a given patient even as it can affect the properties of the obtained material such as surface topography or surface mechanical properties that further may influence biocompatibility. The early phase of basic research included cytotoxicity studies with determination of lactate dehydrogenase activity levels and analysis of surface topography using light and electron microscopy. Substrate samples and their modifications were also subjected to nanoindentation tests: indentation hardness and Vickers hardness. Besides, indentation Young's modulus was determined.

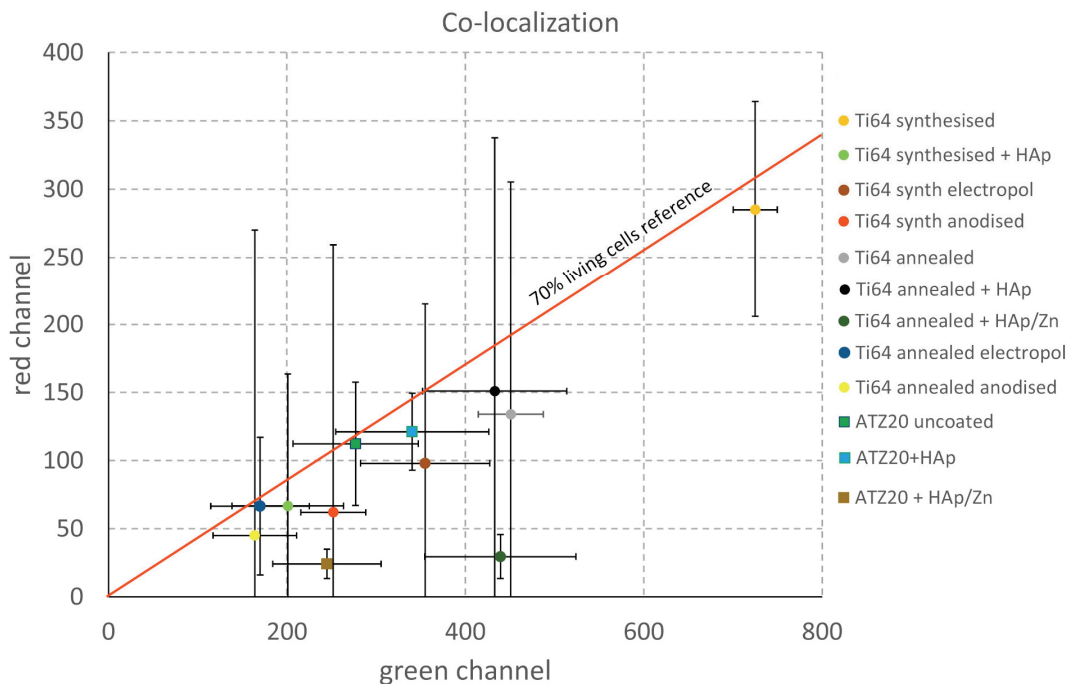


Fig. 8. Co-localization chart of the green and red channels. Lower right part of graph indicates lower cytotoxic effect whereas upper left part stands for more cytotoxic effect. Green channel – live cells, red channel – dead cells

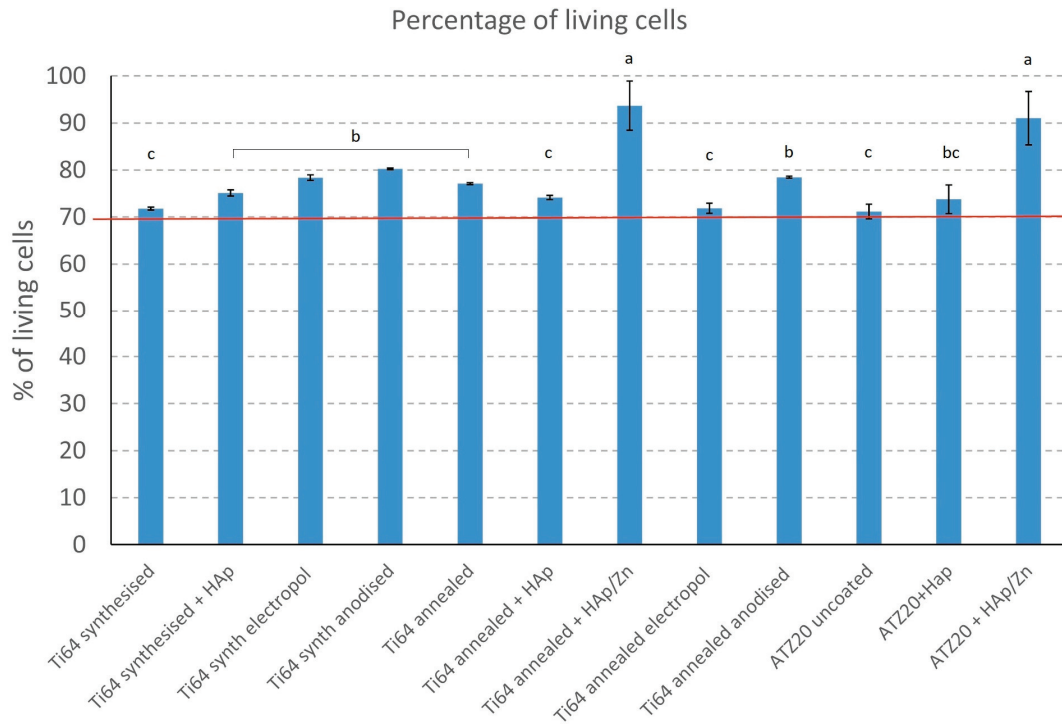


Fig. 9. Percentage of live cells assessed on the basis of mitochondrial activity in relation to all cells on the surface

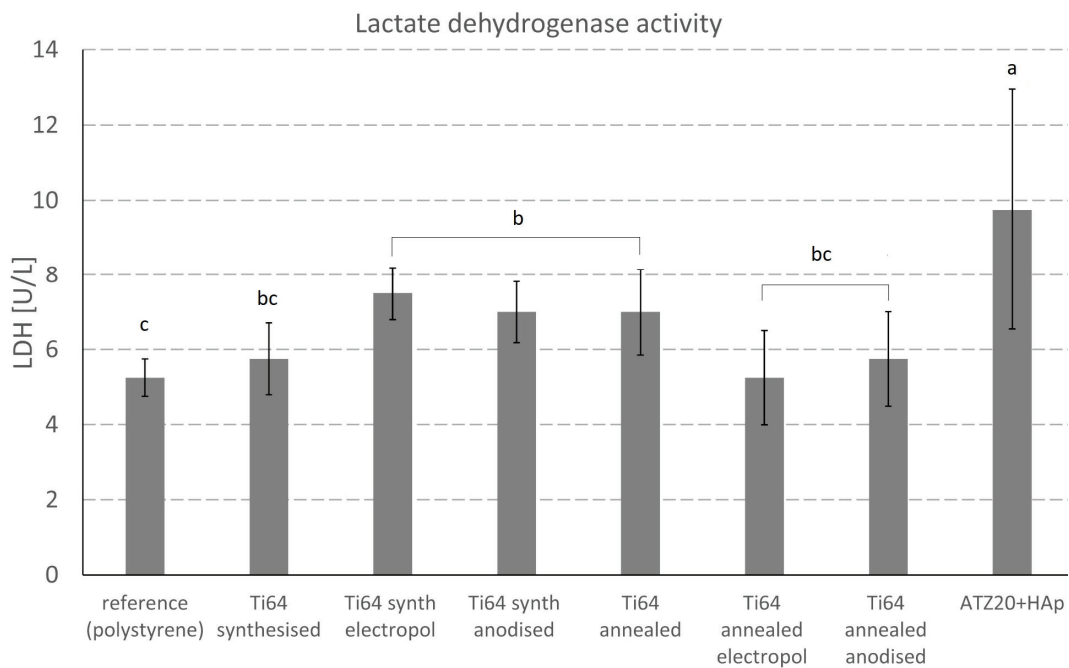


Fig. 10. Cytotoxicity analysis based on the activity of the released lactate dehydrogenase isoenzyme after 24 hours of incubation

### 4.1. Surface modification

The substrate material for the finger bone substitute was the Ti64 alloy, characterized by good biocompatible and mechanical properties as well as high corrosion resistance. Material dedicated to replace the

movable part of the finger (joint) is planned to be made of ATZ20, i.e., the mixture of alumina (20%) and zirconia (80%) characterized by high abrasion resistance and low cytotoxicity. Simultaneously, several methods of surface modification were selected in order to improve the properties of the tested materials, such as hydroxyapatite (HAp) and zinc (HAp/Zn) ar-

gon plasma coating, anodisation, electropolishing and heat treatment. The aim of the electropolishing is to shape the surface roughness, as literature data show, it is the most important reason for bacterial adhesion. The electrolytic polishing process can remove the burrs on the surface and make the metal surface smoother [48]. Anodized titanium has bioactive and ossified surface, which promotes rapid bone integration [1].

## 4.2. Surface topography

Surface modifications of the materials were at first investigated using light microscopy. On a macroscale, the surface of Ti64 is usually greyish silver. However, under the influence of high temperature ( $> 600\text{ }^{\circ}\text{C}$ ) the surface changes its color due to the formation of titanium oxide layers. The annealing of the samples took place in an argon furnace, nevertheless they were cooled in atmospheric air, which allowed the surface to oxidize. This process resulted in obtaining surfaces with different colors, which was caused by the interference of light taking place in layers of titanium oxide of different thicknesses. The much thicker anodized samples were found to have turned blue. That was a direct result of the process parameters that decide on a particular thickness of the titanium oxide layer. The applied voltage of 28 V resulted in the formation of a layer with a thickness of about 60 nm – 75 nm. Electropolishing was aimed at smoothing the surface of the material. The effects of this process were also visible under the microscope as a blurred image of the surface. Hydroxyapatite on the surface of the materials was seen as gray. In addition, introduced zinc particles were visible as silver spots.

Surface modifications strongly affected tested surface topography parameters: surface roughness (Ra) and mean maximum height of the profile (Rz). Ra corresponds to the arithmetic average of the roughness profile and is crucial regarding biological properties and considering the destination of examined samples. Rz parameter is often used to evaluate whether protruding peaks are found on the tested surface. Such peaks can impact direct contact between implant surface and bone. Mean surface roughness and mean maximum height of the profile of uncoated and annealed 3D-printed Ti64 was close to that from the literature [13], [19], [21], [43]. Electropolishing significantly lowered mean Ra and Rz values, compared to results obtained by Zhang [50]. It should be pointed that starting roughness was influencing the final ones – polishing annealed Ti64 resulted in lower Ra and Rz values than raw one. On the

contrary, anodisation increased the arithmetic average of the roughness profile and mean maximum height of the profile; anodisation of annealed sample resulted in higher Ra and Rz values than as-synthesised one. The mean surface roughness and mean maximum height of the profile of the HAp and HAp/Zn coatings on the Ti64 and ATZ20 samples were comparable to results found in literature [40].

SEM observations of uncoated Ti64 showed that the powder particles used for the printing procedure were partially melted. Hydroxyapatite coating formed scaffold-like structures on the surface of Ti64. As a result of anodic oxidation the layers of  $\text{TiO}_2$  formed a smooth film and island-like structures. No typical nanotube structures were observed using given magnification [16]. The cracks present on HAp coated ATZ20 sample may be the result of internal stress caused by plasma spraying [42]. The presence of twins, being the most common deformation mechanisms in hcp metals, that increases their mechanical properties was confirmed. The fine-crystalline layer observed at the surface was the result of surface oxidation and formation of titanium nitrides. Similar structures over the Ti6Al4V alloy were reported in literature on numerous cases [4], [5], [14], [27].

The XRD pattern of Ti64 routinely given in literature [34], usually documents the presence of  $\alpha$ -hcp Ti phase, as the  $\beta$ -bcc Ti is a minor one and their lines partly overlap with the former. The  $\alpha$ - $\text{Al}_2\text{O}_3$  alumina is of tetragonal structure, while the  $\text{ZrO}_2$  takes various crystalline forms: monoclinic below  $1\ 170\text{ }^{\circ}\text{C}$ , tetragonal in temperature range between  $1\ 170\text{ }^{\circ}\text{C}$  and  $2\ 370\text{ }^{\circ}\text{C}$ , followed by bcc above  $2\ 370\text{ }^{\circ}\text{C}$ . Tested samples were sintered at  $1\ 550\text{ }^{\circ}\text{C}$ , and accordingly the tetragonal  $\text{ZrO}_2$  structure was found having a proper backing in the literature data [2], [29], [46].

## 4.3. Micromechanical properties

The mechanical properties of the materials cannot be overlooked in the context of bone implant applications. A material that differs significantly from bone in mechanical terms will result in incorrect load transfer and bone damage [38]. Hardness and Young's modulus of as-synthesised and annealed Ti64 were comparable to human bone [7], [10]. Obtained values of hardness for ATZ20 are comparable to the ones of such samples tested by Maji [29]. HAp coating turned out to be relatively soft, but on the other side anodised and electropolished samples are harder than other Ti64 samples due to titanium oxide layer formation [45]. As-synthesised ATZ20 is also much harder than Ti64

specimens. Additionally, EiT values of Ti64 and ATZ20 did not differ from data found in literature [8], [15]. EiT and HiT values of Ti64 were also confirmed by Ryniewicz [33] and Fotovvati [15]. Measured values of Young's modulus are correlated with hardness – harder samples show higher Young's modulus values. Vickers hardness for typical Ti64 alloy is about 350 HV, whereas for human bones is less than 80 HV. Tested samples that were coated with HAp also showed values comparable with human bone surface.

#### 4.4. Cytotoxicity

HAp/Zn coating proved to have increased the number of live cells. Additionally, zinc doped into coating reacts with oxygen forming zinc oxide (ZnO) which is known for having biocompatible properties [35]. For most of tested samples, besides HAp coated ATZ20, obtained results of cell viability and lactate dehydrogenase activity do not significantly exceed control level and are comparable with literature results [17], [20]. However, HAp/Zn coating significantly increased the cell survivability by more than 10%. Hence, it was concluded that the samples were suitable for *in vivo* toxicity tests.

However, these *in vitro* results are to be evaluated in more extensive *in vivo* studies in the near future. Additionally, there are other factors that influence the development of the material into the implant such as osteointegration, cell mineralization, antibacterial properties and others.

### 5. Conclusions

The surface modifications of 3D printed Ti64 and ATZ20 samples resulted in various surface topographies (presence of oxides, roughness, defects) as well as mechanical properties. Hydroxyapatite coating lowered tested surface roughness parameters, hardness and Young's modulus. On the contrary, anodisation and electropolishing increased hardness and Young's modulus while increasing (anodizing) or lowering (electropolishing) tested surface roughness parameters. XRD analysis confirmed the presence of Titanium, Zirconia and Alumina phases in the tested samples. Furthermore, titanium, aluminum and zirconium oxides were found on their surfaces. Cytotoxicity analysis showed that the samples had no cytotoxic effect. Besides, HAp/Zn coating increased cell viability from 77% to 91% for uncoated annealed Ti64 and from 75%

to 94% for uncoated ATZ20. The HAp coating itself did not increase the cell viability in a significant way. In brief, all of tested biomaterials had fulfill basic finger implants requirements and are suitable for future *in vitro* and *in vivo* studies since materials intended for contact with human tissues need in-depth research. Concerning *in vivo* experiments, the *in vitro* analysis is insufficient to prove the materials' cytocompatibility, thus, at this level of the project execution, small animal models were considered in particular for testing the general dermal toxicity. The further studies mostly with osteoblast cells, including cytotoxicity and mineralization studies will be the subject of the further test and will enable the submission of a proposal for studies in large animal models.

#### Author's contribution

- A. The preparation of the research program: R. Major, K. Kasperkiewicz, J.M. Lackner, D.B. Lumenta;
- B. The execution of research: A. Byrski, Ł. Major, M. Dyrner, J. M. Lackner;
- C. The statistical analysis: A. Byrski;
- D. The interpretation of data: M. Kopernik, Ł. Major, D.B. Lumenta;
- E. Preparation of the manuscript: A. Byrski, K. Kasperkiewicz, R. Major, M. Kopernik;
- F. Obtain financing: R. Major, J.M. Lackner, M. Kopernik.

#### Declaration of competing interest

The authors declare that they have no known competing financial interests or personal relationships that could have appeared to influence the work reported in this paper.

#### Acknowledgements

This research was financially supported by the Polish National Centre of Research and Development (Grant no. fingerIMPLANT M-ERA.NET2/2019/7/2020, "Patient-specific, anti-microbial bioactive finger implants for durable functional reconstruction after amputation") and the Austrian Research and Promotion Agency (FFG), Grant no. 878515. The part of paper was financed by the Ministry of Science and Education (AGH University of Krakow statutory research project No. 16.16.110.663). Further support was granted by FFG within the BRIDGE Young Scientists programme by the project "safeFACEimplant" (Grant no. 872667).

The Austrian company partner Martin Schwentenwein (Lithoz GmbH) is acknowledged for providing the ATZ samples.

#### References

- [1] ALIPAL J., LEE T.C., KOSHY P., ABDULLAH H.Z., IDRIS M.I., *Evolution of anodised titanium for implant applications*, Heliyon, 2021, 7, DOI: 10.1016/J.HELIYON.2021.E07408.

- [2] AMAT N.F., MUCHTAR A., AMRIL M.S., GHAZALI M.J., YAHAYA N., *Effect of sintering temperature on the aging resistance and mechanical properties of monolithic zirconia*, *J. Mater. Res. Technol.*, 2019, 8, 1092–1101, DOI: 10.1016/J.JMRT.2018.07.017.
- [3] ARCOS D., VALLET-REGÍ M., *Substituted hydroxyapatite coatings of bone implants*, *J. Mater. Chem. B.*, 2020, 8, 1781–1800, DOI: 10.1039/C9TB02710F.
- [4] BARRIOBERO-VILA P., GUSSONE J., HAUBRICH J., SANDLÖBES S., DA SILVA J.C., CLOETENS P., SCHELL N., REQUENA G., *Inducing Stable  $\alpha + \beta$  Microstructures during Selective Laser Melting of Ti-6Al-4V Using Intensified Intrinsic Heat Treatments*, *Mater.*, 2017, 10: 268, DOI: 10.3390/MA10030268.
- [5] BARRIOBERO-VILA P., GUSSONE J., STARK A., SCHELL N., HAUBRICH J., REQUENA G., *Peritectic titanium alloys for 3D printing*, *Nat. Commun.*, 2018, 9, 1–9, DOI: 10.1038/s41467-018-05819-9.
- [6] BERGAMO E.T.P., CARDOSO K.B., LINO L.F.O., CAMPOS T.M.B., MONTEIRO K.N., CESAR P.F., GENOVA L.A., THIM G.P., COELHO P.G., BONFANTE E.A., *Alumina-toughened zirconia for dental applications: Physicochemical, mechanical, optical and residual stress characterization after artificial aging*, *J. Biomed. Mater. Res. B. Appl. Biomater.*, 2021, 109, 1135–1144, DOI: 10.1002/JBM.B.34776.
- [7] BISWAS S., DASGUPTA P., PRAMANIK P., CHANDA A., *Macro and Micro-indentation Behavior of the Cortical Part of Human Femur*, *Procedia Mater. Sci.*, 2014, 5: 2320–2329, DOI: 10.1016/J.MSPRO.2014.07.475.
- [8] BORGES L., GELFI M., BONTEMPI E., GOUDEAU P., GEANDIER G., THIAUDIÈRE D., DEPERO L.E., *Young modulus and Poisson ratio measurements of TiO<sub>2</sub> thin films deposited with Atomic Layer Deposition*, *Surf. Coatings Technol.*, 2012, 206, 2459–2463, DOI: 10.1016/J.SURFCOAT.2011.10.050.
- [9] CHEN K., ZHOU G., LI Q., TANG H., WANG S., LI P., GU X., FAN Y., *In vitro degradation, biocompatibility and antibacterial properties of pure zinc: assessing the potential of Zn as a guided bone regeneration membrane*, *J. Mater. Chem. B.*, 2021, 9, 5114–5127, DOI: 10.1039/D1TB00596K.
- [10] DALL'ARA E., GRABOWSKI P., ZIOUPOS P., VICECONTI M., *Estimation of local anisotropy of plexiform bone: Comparison between depth sensing micro-indentation and Reference Point Indentation*, *J. Biomech.*, 2015, 48, 4073–4080, DOI: 10.1016/J.JBIOMECH.2015.10.001.
- [11] DILEEP KUMAR V.G., SRIDHAR M.S., ARAMWIT P., KRUT'KO V.K., MUSSKAYA O.N., GLAZOV I.E., REDDY N., *A review on the synthesis and properties of hydroxyapatite for biomedical applications*, *J. Biomater. Sci. Polym. Ed.*, 2022, 33, 229–261, DOI: 10.1080/09205063.2021.1980985.
- [12] ELBEHRY A., AL-DUBAIB M., MARZOUK E., MOUSSA I., *Antibacterial effects and resistance induction of silver and gold nanoparticles against Staphylococcus aureus-induced mastitis and the potential toxicity in rats*, *Microbiologyopen*, 2019, 8, e00698, DOI: 10.1002/mbo3.698.
- [13] ERIC W., CLAUS E., SHAFQAAT S., FRANK W., *High Cycle Fatigue (HCF) Performance of Ti-6Al-4V Alloy Processed by Selective Laser Melting*, *Adv. Mater. Res.*, 2013, 816–817, 134–139, DOI: 10.4028/WWW.SCIENTIFIC.NET/AMR.816-817.134.
- [14] FARABI E., TARI V., HODGSON P.D., ROHRER G.S., BELADI H., *On the grain boundary network characteristics in a martensitic Ti-6Al-4V alloy*, *J. Mater. Sci.*, 2020, 55, 15299–15321, DOI: 10.1007/S10853-020-05075-7/FIGURES/12.
- [15] FOTOVVATI B., NAMDARI N., DEGHANGHADIKOLAEI A., DAI N., ZHANG J., CHEN Y., GONG H., DILIP J.S., YANG L., TENG C., STUCKER B., *Influence of small particles inclusion on selective laser melting of Ti-6Al-4V powder*, *IOP Conf. Ser. Mater. Sci. Eng.*, 2017, 272, 012024, DOI: 10.1088/1757-899X/272/1/012024.
- [16] FOUSOVÁ M., VOJTĚCH D., KUBÁSEK J., JABLONSKÁ E., FOJT J., *Promising characteristics of gradient porosity Ti-6Al-4V alloy prepared by SLM process*, *Mech. Behav. Biomed. Mater.*, 2017, 69, 368–376, DOI: 10.1016/J.JMBB.2017.01.043.
- [17] GINESTRA P., FERRARO R.M., ZOHAR-HAUBER K., ABENI A., GILIANI S., CERETTI E., *Selective Laser Melting and Electron Beam Melting of Ti6Al4V for Orthopedic Applications: A Comparative Study on the Applied Building Direction*, *Mater.*, 2020, 13, 5584, DOI: 10.3390/MA13235584.
- [18] GOEL S., BJÖRKLUND S., CURRY N., GOVINDARAJAN S., WIKLUND U., GAUDIUSO C., JOSHI S., *Axial Plasma Spraying of Mixed Suspensions: A Case Study on Processing, Characteristics, and Tribological Behavior of Al<sub>2</sub>O<sub>3</sub>-YSZ Coatings*, *Appl. Sci.*, 2020, 10, 5140, DOI: 10.3390/APP10155140.
- [19] GREITEMEIER D., DALLE DONNE C., SYASSEN F., EUFINGER J., MELZ T., *Effect of surface roughness on fatigue performance of additive manufactured Ti-6Al-4V*, *Mater. Sci. Technol.*, (United Kingdom), 2016, 32, 629–634, DOI: 10.1179/1743284715Y.0000000053.
- [20] HAN X., GELEIN R., CORSON N., WADE-MERCER P., JIANG J., BISWAS P., FINKELSTEIN J.N., ELDER A., OBERDÖRSTER G., *Validation of an LDH assay for assessing nanoparticle toxicity*, *Toxicology*, 2011, 287, 99–104, DOI: 10.1016/J.TOX.2011.06.011.
- [21] KAHLIN M., ANSELL H., MOVERARE J.J., *Fatigue behaviour of notched additive manufactured Ti6Al4V with as-built surfaces*, *Int. J. Fatigue*, 2017, 101, 51–60, DOI: 10.1016/J.IJFATIGUE.2017.04.009.
- [22] KANG JIE J., XU SHI B., WANG DOU H., WANG BIAO C., ZHU NA L., *Delamination failure monitoring of plasma sprayed composite ceramic coatings in rolling contact by acoustic emission*, *Eng. Fail Anal.*, 2018, 86, 131–141, DOI: 10.1016/J.ENGFAILANAL.2018.01.005.
- [23] KASPERKIEWICZ K., MAJOR R., SYPIEN A., KOT M., DYNER M., MAJOR L., BYRSKI A., KOPERNIK M., LACKNER J.M., *Antibacterial Optimization of Highly Deformed Titanium Alloys for Spinal Implants*, *Molecules*, 2021, 26, DOI: 10.3390/MOLECULES26113145.
- [24] KHATOON Z., MCTIERNAN C.D., SUURONEN E.J., MAH T.F., ALARCON E.I., *Bacterial biofilm formation on implantable devices and approaches to its treatment and prevention*, *Heliyon*, 2018, 4, 1067, DOI: 10.1016/j.heliyon.2018.e01067.
- [25] KOMASA S., KUSUMOTO T., HAYASHI R., TAKAO S., LI M., YAN S., ZENG Y., YANG Y., HU H., KOBAYASHI Y., AGARIGUCHI A., NISHIDA H., HASHIMOTO Y., OKAZAKI J., *Effect of Argon-Based Atmospheric Pressure Plasma Treatment on Hard Tissue Formation on Titanium Surface*, *Int. J. Mol. Sci.*, 2021, 22, 7617, DOI: 10.3390/IJMS22147617.
- [26] LI W., LIU W., LI M., NIE J., CHEN Y., XING Z., *Nanoscale Plasticity Behavior of Additive-Manufactured Zirconia-Toughened Alumina Ceramics during Nanoindentation*, *Mater.* (Basel, Switzerland), 2020, 13, DOI: 10.3390/MA13041006.
- [27] LIU H.J., ZHOU L., LIU P., LIU Q.W., *Microstructural evolution and hydride precipitation mechanism in hydrogenated Ti-6Al-4V alloy*, *Int. J. Hydrogen Energy*, 2009, 34, 9596–9602, DOI: 10.1016/J.IJHYDENE.2009.09.098.
- [28] LUO Q., CAO H., WANG L., MA X., LIU X., *ZnO@ZnS nanorod-array coated titanium: Good to fibroblasts but bad to bacteria*, *J. Colloid Interface Sci.*, 2020, 579, 50–60, DOI: 10.1016/J.JCIS.2020.06.055.

- [29] MAJI A., CHOUBEY G., *Microstructure and Mechanical Properties of Alumina Toughened Zirconia (ATZ)*, Mater Today Proc., 2018, 5, 7457–7465, DOI: 10.1016/J.MATPR.2017.11.417.
- [30] MICHELETTI C., LEE B.E.J., DEERING J., BINKLEY D.M., COULSON S., HUSSANAIN A., ZUROB H., GRANDFIELD K., *Ti-5Al-5Mo-5V-3Cr bone implants with dual-scale topography: a promising alternative to Ti-6Al-4V*, Nanotechnology, 2020, 31, DOI: 10.1088/1361-6528/AB79AC.
- [31] MINKIEWICZ-ZOCHNIAK A., JARZYŃKA S., IWAŃSKA A., STROM K., IWAŃCZYK B., BARTEL M., MAZUR M., PIETRUCZUK-PADZIK A., KONIECZNA M., AUGUSTYNOWICZ-KOPEĆ E., OŁĘDZKA G., *Biofilm formation on dental implant biomaterials by staphylococcus aureus strains isolated from patients with cystic fibrosis*, Materials, (Basel), 2021, 14, DOI: 10.3390/ma14082030.
- [32] ROSETI L., PARISI V., PETRETTA M., CAVALLO C., DESANDO G., BARTOLOTTI I., GRIGOLO B., *Scaffolds for Bone Tissue Engineering: State of the art and new perspectives*, Mater. Sci. Eng. C. Mater. Biol. Appl., 2017, 78, 1246–1262, DOI: 10.1016/J.MSEC.2017.05.017.
- [33] RYŃNIEWICZ A.M., BOJKO Ł., RYŃNIEWICZ W.I., *Microstructural and micromechanical tests of titanium biomaterials intended for prosthetic reconstructions*, Acta Bioeng. Biomech., 2016, 18, 111–117, DOI:10.5277/ABB-00193-2014-02.
- [34] SARKER A., TRAN N., RIFAI A., BRANDT M., TRAN P.A., LEARY M., FOX K., WILLIAMS R., *Rational design of additively manufactured Ti6Al4V implants to control Staphylococcus aureus biofilm formation*, Materialia, 2019, 5, 100250, DOI: 10.1016/J.MTLA.2019.100250.
- [35] SHIMABUKURO M., TSUTSUMI Y., NOZAKI K., CHEN P., YAMADA R., ASHIDA M., DOI H., NAGAI A., HANAWA T., *Chemical and Biological Roles of Zinc in a Porous Titanium Dioxide Layer Formed by Micro-Arc Oxidation*, Coatings, 2019, 9, 705, DOI: 10.3390/COATINGS9110705.
- [36] SHU T., ZHANG Y., SUN G., PAN Y., HE G., CHENG Y., LI A., PEI D., *Enhanced Osseointegration by the Hierarchical Micro-Nano Topography on Selective Laser Melting Ti-6Al-4V Dental Implants*, Front. Bioeng. Biotechnol., 2021, 8, DOI: 10.3389/FBIOE.2020.621601.
- [37] SOUZA J.G.S., BERTOLINI M.M., COSTA R.C., NAGAY B.E., DONGARI-BAGTZOGLU A., BARÃO V.A.R., *Targeting implant-associated infections: titanium surface loaded with antimicrobial*, iScience, 2021, 24, 102008, DOI: 10.1016/J.ISCI.2020.102008.
- [38] STĘPNIEWSKI A.A., *Analysis of fatigue loads of the knee joint during gait*, Acta Bioeng. Biomech. Orig. Pap., 2019, 21, DOI: 10.5277/ABB-01387-2019-03.
- [39] SU X., WANG T., GUO S., *Applications of 3D printed bone tissue engineering scaffolds in the stem cell field*, Regen Ther., 2021, 16, 63–72, DOI: 10.1016/J.RETH.2021.01.007.
- [40] TOMALA A.M., SŁOTA D., FLORKIEWICZ W., PIĘTAK K., DYLAG M., SOBCZAK-KUPIEC A., *Tribological Properties and Physiochemical Analysis of Polymer-Ceramic Composite Coatings for Bone Regeneration*, Lubr., 2022, 10, 58, DOI: 10.3390/LUBRICANTS10040058.
- [41] VALTANEN R.S., YANG Y.P., GURTNER G.C., MALONEY W.J., LOWENBERG D.W., *Synthetic and Bone tissue engineering graft substitutes: What is the future?*, Injury, 2021, 52, S72–S77, DOI: 10.1016/J.INJURY.2020.07.040.
- [42] VARGHESE G., MORAL M., CASTRO-GARCÍA M., LÓPEZ-LÓPEZ J.J., MARÍN-RUEDA J.R., YAGÜE-ALCARAZ V., HERNÁNDEZ-AFONSO L., RUIZ-MORALES J.C., CANALES-VÁZQUEZ J., *Fabrication and characterisation of ceramics via low-cost DLP 3D printing*, Boletín la Soc Española Cerámica y Vidr, 2018, 57, 9–18, DOI: 10.1016/J.BSECV.2017.09.004.
- [43] WANG M., WU Y., LU S., CHEN T., ZHAO Y., CHEN H., TANG Z., *Fabrication and characterization of selective laser melting printed Ti-6Al-4V alloys subjected to heat treatment for customized implants design*, Prog. Nat. Sci. Mater. Int., 2016, 26, 671–677, DOI: 10.1016/j.pnsc.2016.12.006.
- [44] WANG Z., WANG X., WANG Y., ZHU Y., LIU X., ZHOU Q., *NanoZnO-modified titanium implants for enhanced antibacterial activity, osteogenesis and corrosion resistance*, J. Nanobiotechnology, 2021, 19, DOI: 10.1186/S12951-021-01099-6.
- [45] WOJCIESZAK D., MAZUR M., INDYKA J., JURKOWSKA A., KALISZ M., DOMANOWSKI P., KACZMAREK D., DOMARADZKI J., *Mechanical and structural properties of titanium dioxide deposited by innovative magnetron sputtering process*, Mater. Sci. Pol., 2015, 33, 660–668, DOI: 10.1515/MSP-2015-0084.
- [46] XIE S., GUO L., ZHANG M., QIN J., HU R., *Durable hydrophobic ceramics of Al<sub>2</sub>O<sub>3</sub>-ZrO<sub>2</sub> modified by hydrophilic silane with high oil/water separation efficiency*, J. Porous Mater., 2021, 284 (28), 1115–1127, DOI: 10.1007/S10934-021-01055-7.
- [47] YABUTSUKA T., KIDOKORO Y., TAKAI S., *Improvement of hydroxyapatite formation ability of titanium-based alloys by combination of acid etching and apatite nuclei precipitation*, IET Nanobiotechnology, 2020, 14, 688–694, DOI: 10.1049/IET-NBT.2020.0053.
- [48] YANG L., LASSELL A., PAIVA G., *Further study of the electropolishing of Ti 6 Al 4 V parts made via electron beam melting*, Mater. Sci., 2015, 1730–1737.
- [49] ZANDINEJAD A., REVILLA-LEÓN M., METHANI M.M., KHANLAR L.N., MORTON D., *The Fracture Resistance of Additively Manufactured Monolithic Zirconia vs. Bi-Layered Alumina Toughened Zirconia Crowns When Cemented to Zirconia Abutments. Evaluating the Potential of 3D Printing of Ceramic Crowns: An In Vitro Study*, Dent. J., 2021, 9, DOI: 10.3390/DJ9100115.
- [50] ZHANG Y., LI J., CHE S., *Electrochemical Science Electropolishing Mechanism of Ti-6Al-4V Alloy Fabricated by Selective Laser Melting*, Int. J. Electrochem. Sci., 2018, 13, 4792–4807, DOI: 10.20964/2018.05.79.